# Transition fibre protein FBF1 is required for the ciliary entry of assembled intraflagellar transport complexes

**Qing Wei**[1], **Qingwen Xu**[3], **Yuxia Zhang**[1], **Yujie Li**[1], **Qing Zhang**[1], **Zeng Hu**[1], **Peter C. Harris**[1,2], **Vicente E. Torres**[1,2], **Kun Ling**[2,3,†], and **Jinghua Hu**[1,2,3,†]

[1]Division of Nephrology and Hypertension, Mayo Clinic, Rochester, Minnesota, USA

[2]Mayo Translational PKD Center, Rochester, Minnesota, USA

[3]Department of Biochemistry and Molecular Biology, Mayo Clinic, Rochester, Minnesota, USA

## Abstract

Sensory organelle cilia play critical roles in mammalian embryonic development and tissue homeostasis. Intraflagellar transport (IFT) machinery is required for the assembly and maintenance of cilia. Yet how this large complex passes through the size-dependent barrier at the ciliary base remains enigmatic. Here we report that FBF1, a highly conserved transition fibre protein, is required for the ciliary import of assembled IFT particles at the cilia base. We cloned *dyf-19*, the *C. elegans* homolog of human *FBF1*, in a whole-genome screen for ciliogenesis mutants. DYF-19 localizes specifically to transition fibres and interacts directly with the IFT-B component DYF-11/IFT54. Although not a structural component of transition fibres, DYF-19 is essential for the transit of assembled IFT particles through the ciliary base. Furthermore, we found that human FBF1 shares conserved localization and function with its worm counterpart. We conclude that FBF1 is a key functional transition fibre component that facilitates the ciliary entry of assembled IFT machinery.

## Introduction

Primary cilia exist on most eukaryotic cell surfaces and function as the cell's antenna to transduce many critical cellular signaling pathways[1, 2]. Cilia dysfunction has been linked to a wide spectrum of human genetic diseases, collectively known as ciliopathies[3, 4]. Consistent with the ubiquitous presence of cilia on the surfaces of most cells in the human body, most ciliopathies occur as syndromic disorders that affect the homeostasis of many

organs during development, including the kidneys, liver, limbs, eyes, central nervous system (CNS), and fat storage tissue.

Intraflagellar transport (IFT) complexes are an evolutionarily conserved machinery that move bidirectionally from the ciliary base to the tip to transport cargos required for ciliogenesis and signaling[5, 6, 7, 8]. The IFT machinery comprises >20 proteins, including motors, IFT-A subcomplexes, IFT-B subcomplexes and the BBSome[5, 6, 7, 8]. Many structural components of the IFT machinery are large proteins with size >60 kDa. Additionally, some IFT cargoes, such as radial spokes and dynein arms, are also pre-assembled in the cytoplasm prior to their ciliary entry[9, 10]. How these large proteins and complexes pass through the recently reported size-dependent barrier at the ciliary base remains poorly understood[11, 12].

Ultrastructural studies have shown that the morphology of the ciliary base is highly conserved, including a basal body (transformed from the mother centriole), transition fibres (TFs, transformed from the distal appendages of the mother centriole), and the transition zone (TZ, the proximal part of the axoneme that contains Y-links)[13]. TFs form a nine-bladed propeller-like structure of unknown protein composition and connect the distal end of the basal body to the ciliary membrane [14]. Above TFs, the Y-links of the TZ connect the proximal segments of axonemal microtubules to the ciliary membrane[15]. Recently, emerging evidence suggests that many proteins mutated in human ciliopathy syndromes specifically localize around the TZ and probably form a multimeric protein complex to regulate the integrity of Y-links and/or the ciliary entry of some ciliary proteins[16, 17, 18, 19, 20, 21, 22]. In drastic contrast, little is known about the molecular identity and function of TFs in the context of cilia.

The observations that IFT components concentrate around TFs in the preciliary compartment led to the hypothesis that TFs might be a critical site for the docking or sorting of IFT particles or individual components before they enter the cilium[23]. However, none of the identified distal appendage proteins have been shown to regulate the ciliary import or sorting of IFT particles or individual components associated with TFs[24, 25, 26, 27]. In a whole-genome genetic screen for *C. elegans* mutants with disrupted IFT integrity, we retrieved and cloned *dyf-19*, the homolog of human *FBF1*. Both DYF-19 and FBF1 are poorly characterized proteins. DYF-19 specifically localizes to TFs and is essential for the ciliary entry of IFT complexes through direct interaction with IFT-B component DYF-11 (the ortholog of human IFT54). DYF-19 deficiency does not affect TF assembly but results in the accumulation of assembled IFT particles below TFs. Furthermore, we found that human FBF1 is essential for ciliogenesis and shares conserved specific TF localization and function with its worm counterpart. Collectively, our findings demonstrate that FBF1 defines the TFs as the key site for regulating the ciliary entry of assembled IFT machinery.

## Results

### TF protein DYF-19 regulates ciliogenesis in *C. elegans*

To search for mutant nematodes with abnormal ciliogenesis, we performed a genome-wide ethyl methanesulfonate (EMS) mutagenesis screen in *C. elegans*. From this screen, we

cloned a novel mutant, *dyf-19*. In *C. elegans*, mutants with abnormal ciliogenesis cannot take up fluorescent dye and are thus called dye-filling defective (Dyf) [28]. *dyf-19* encodes Y43F8C.4, which is the homolog of human FBF1 [Fas (TNFRSF6)-binding factor 1)] protein [29] (Fig. 1a, Supplementary Fig. S1a). Originally identified as a keratin filament-binding protein[30], FBF1 shows asymmetric centrosome localization[31] and was recently confirmed as one of the distal appendage proteins (DAPs)[25], but with uncharacterized function. Our bioinformatics analyses indicate that FBF1 is the only DAP identified so far (CEP164, CEP89, CEP83, SCLT1, FBF1[25]) with a clear homolog in worm genome. This suggests that FBF1 probably plays a highly conserved and important role on TFs. *dyf-19* mutants possessed truncated cilia and exhibited abnormal accumulation of the IFT-B component OSM-6 (the ortholog of human IFT52) at the residual cilia tip (Fig. 1b, c). Few or no IFT movements were observed in *dyf-19* cilia. Introducing a wild-type *Y43F8C.4* gene fully rescued the ciliogenesis defect in *dyf-19* mutants (Fig. 1c, d).

Promoter expression analysis demonstrated that *dyf-19* is expressed exclusively in ciliated cells (Supplementary Fig. S1b). At the *C. elegans* ciliary base, the periciliary membrane trafficking compartment (PCMC) was found immediately below the TFs[32], and the transition zone (TZ) was located just above the TFs [13] (Fig. 1g). mCherry-tagged DYF-19 was found to localize above the PCMC marker GFP-tagged RPI-2 (the worm homolog of human X-linked retinitis pigmentosa 2 (RP2)), but below the TZ markers GFP-tagged NPHP-1 or MKS-5 in the cilia, indicating that DYF-19 is a genuine TF component (Fig. 1e–g). Truncated DYF-19[1–294], encoded by the *jhu455* allele used in our experiments, failed to target cilia and accumulated only in cell bodies (Fig. 1a, Supplementary Fig. S1c), suggesting that *dyf-19(jhu455)* is functionally null. The observation that *dyf-19(jhu455)* worms still possess normal TFs at the ciliary base indicates that DYF-19 is a functional, but not structural, component of TFs (Fig. 1h).

## The function of DYF-19 is independent of the TZ

TFs and the TZ are spatially located adjacent to each other. The TZ is thought to restrict the ciliary entry of some nonciliary proteins[20]. We observed no abnormality in either the localization of TZ proteins or the morphology of TZ Y-links in *dyf-19* mutants (Supplementary Fig. S2a, b). It was reported that MKS and NPHP modules cooperate to establish a functional TZ[20, 33, 34, 35]. In *C. elegans*, cilia exist at the tips of dendrites in ciliated sensory neurons. The combination of any *mks* mutant with an *nphp* mutant will disrupt TZ function and result in severely truncated dendrites due to perturbed anchoring of basal bodies [20, 33, 34]. Unlike *mks-6; nphp-1* mutants, *dyf-19; mks-6* or *dyf-19; nphp-1* double mutants possessed well-formed dendrites (Supplementary Fig. S2c), indicating that *dyf-19* does not genetically interact with TZ components.

## DYF-19 is required for the ciliary entry of IFT particles

IFT is indispensable for ciliogenesis. To discern the role of DYF-19, as well as TFs, in IFT regulation, we examined various GFP-tagged IFT components in *dyf-19* mutants. Like OSM-6 (Fig. 1c), other IFT-B components or the IFT-B–associated kinesin motor OSM-3 (the ortholog of human KIF17) accumulated at the tips of truncated *dyf-19* cilia (Fig. 2a) and showed little or no IFT motility. In striking contrast, the IFT-A component CHE-11 (the

ortholog of human IFT140), IFT-A–associated kinesin-II motor KAP-1, IFT retrograde motor dynein light chain XBX-1 (the ortholog of human D2LIC), and BBSome components lost their ciliary presence in *dyf-19* mutants (Fig. 2a). The ciliary absence of the IFT-A subcomplex and dynein (key players in the retrograde IFT machinery [36, 37, 38, 39, 40, 41]) and of the BBSome[42, 43] (key players in IFT assembly[44, 45, 46, 47]) explains the ciliary accumulation of IFT-B components. We further found that IFT-A and BBSome proteins were restricted below TFs in *dyf-19* cilia, suggesting that their ability to pass through TFs depends on DYF-19 (Fig. 2b–d).

When co-labeling cilia with GFP-tagged CHE-11 (IFT-A) and mCherry-tagged OSM-6 (IFT-B), we noticed that IFT-A and IFT-B still colocalize at the *dyf-19* ciliary base (Fig. 3a). We thus hypothesized that assembled IFT complexes may still exist at the ciliary base but fail to enter the cilium in *dyf-19* mutants. Previously, we successfully applied a bimolecular fluorescence complementation (BiFC) assay to examine IFT integrity in live worms [47]. The BiFC assay was developed to directly visualize protein-protein interactions in the same macromolecular complex in their natural environment[48]. In wt cilia, fluorescence complementation was clearly observed between IFT-A component CHE-11 and IFT-B component IFT-20, between BBSome components BBS-7 and BBS-9, as well as between IFT component DYF-2 (the ortholog of human IFT144) and BBSome component BBS-9, indicating the formation of functional IFT particles (Fig. 3b). The following observations indicate that the complemented IFT protein pairs are functional: they showed characteristic IFT movement (Supplementary Fig. S3a); the fluorescence complementation was disrupted in *ift* mutants (Supplementary Fig. S3b); and they could rescue ciliogenesis defects of corresponding *ift* or *bbs* mutants, respectively (Supplementary Fig. S3c). Notably, consistent with previous observation that IFT components concentrate around TFs[23], we found that the majority of complemented BiFC signal concentrated at a similar site in wt cilia (Fig. 3b–d), suggesting that the area around TFs is the major pool for assembled IFT particles. In contrast, in *dyf-19* mutants, fluorescence complementation was completely restricted to below the TZ (Fig. 3c–d), a site comparable to that where IFT-A and BBSome proteins were found in *dyf-19* mutants (Fig. 2b–d). Furthermore, no IFT movement could be observed for any of the BiFC pairs examined in *dyf-19* cilia. Taken together, these observations suggest that the assembled IFT particles fail to pass through TFs in DYF-19-deficient cilia. Interestingly, individual IFT-B components appear to enter the cilia independently of DYF-19, probably regulated by an unknown TF functional component or by compensatory mechanisms.

## DYF-19 directly interacts with the IFT-B component DYF-11

When we were examining various IFT components in *dyf-19* mutants, DYF-11 (the ortholog of human IFT-B component IFT54) came to our attention. Unlike other IFT-B components (Fig. 2a), small amounts of DYF-11 entered cilia but showed no accumulation, and the majority of DYF-11 was restricted below the TFs (Fig. 4a). This unique mislocalization phenotype was not observed in any other *ift* mutants (Fig. 4a), leading us to suspect that DYF-11 might be the effector of DYF-19 in regulating the ciliary entry of IFT particles. Indeed, we found that DYF-19 interacts directly with the N-terminus of DYF-11 (Fig. 4b). As expected, we visualized strong fluorescence complementation between DYF-19 and

DYF-11 around TFs in the BiFC assay (Fig. 4c). In contrast, we detected no or very weak fluorescence complementation between DYF-19 and other IFT components, either the IFT-A component CHE-11 or the IFT-B component OSM-6, in wt cilia (Fig. 4c). These observations indicate that DYF-11 is probably the adaptor that bridges the IFT particle to DYF-19 around TFs. Moreover, as reported previously [49], we noted that *dyf-11* mutants phenocopy *dyf-19* mutants in that IFT-B components enter truncated cilia, but IFT-A components fail to do so (Fig. 4d). However, the fact that the CHE-11-IFT-20 BiFC signal was totally disrupted in *dyf-11* mutants (Supplementary Fig. S3b), probably due to the role of DYF-11 as an essential IFT structural component, prevented us from further examining whether assembled IFT particles fail to enter DYF-11-deficient cilia. Taken together, our results suggest that the TF component DYF-19 regulates the ciliary entry of assembled IFT particles through a direct interaction with the IFT component DYF-11 (Fig. 4e).

### The localization and function of DYF-19 is highly conserved

Because DYF-19 is conserved between worms and humans, we next asked whether its mammalian homolog, FBF1, plays a similar role. As expected, both endogenous FBF1 and overexpressed, Flag-tagged FBF1 consistently formed a ring-like structure around the mother centriole or at the ciliary base in IMCD3 cells (Fig. 5a–c). On mother centrioles, FBF1 colocalized with the distal appendage protein CEP164[24] and localized above the sub-distal appendage protein ODF2 (Fig. 5d). Immuno-EM analyses confirmed that FBF1 specifically localized along distal appendages of the mother centriole (Fig. 5e). Distal appendages exist only on mother centrioles. Consistently, FBF1 was only restricted to the mother centriole during G1/S and G2 phases of the cell cycle. At the late G2 phase or early M phase, FBF1 started to appear on the other maturing centriole, and the signal increased during subsequent stages of mitosis (Supplementary Fig. S4).

Depletion of FBF1 resulted in severely truncated cilia (Fig. 5f–h). Similar to what we observed in *C. elegans* DYF-19-deficient cilia, the IFT-B component IFT88 but not the IFT-A component IFT140 could enter the truncated cilia (Fig. 5i, j). As expected, we detected a direct interaction between FBF1 and IFT54, the mouse ortholog of worm DYF-11, in a GST pull-down assay (Supplementary Fig. S5). Immunoprecipitation confirmed that endogenous IFT54 associates with either endogenous FBF1 or overexpressed FBF1 (Fig. 5k, l). Further mapping of the interaction indicated that the IFT54 N-terminus (aa 1–325) probably interacts with FBF1 at multiple sites, but with a stronger binding at FBF1 C-terminus (aa 816–1075) (Supplementary Fig. S5).

## Discussion

In summary, FBF1 (or DYF-19) specifically targets to TFs, interacts directly with the IFT component IFT54 (or DYF-11), and plays a role in regulating the passage of assembled IFT particles into the cilium. The highly conserved subcellular localization as well as function across species strongly supports the conclusion that FBF1 (or DYF-19) is a core functional determinant that makes TFs a key site for regulating the ciliary import of assembled IFT machinery.

Since the discovery of the cilium more than a century ago, a central question in cilia biology is how the sensory cilium is functionally separated from the cytosol. At the ciliary base, there is a size-dependent diffusion barrier that restricts the ciliary entry of large proteins[11, 12], indicating that a passive gate selectively regulates the ciliary entry of various ciliogenic proteins. The size of most IFT components is larger than 60 kDa, and the assembled IFT particle is larger than 1 MDa. How the IFT particle or its components actively pass through the ciliary gate remains a mystery. The obvious pore complex formed by Y-links of the TZ at the ciliary base led to the notion that the Y-links probably act as the active ciliary gate[7, 50]. However, the depletion of TZ components causes no major defect in the ciliary entry of IFT particles or of any IFT components[20], indicating that an active gating mechanism functions upstream of the TZ. Our observations suggest that TFs, which form a cartwheel structure just below the TZ, probably form the ciliary gate for IFT machinery. FBF1 (or DYF-19) facilitates the passage of assembled IFT particles through TFs.

It is likely that FBF1 (DYF-19) provides a docking site on TFs for assembled IFT particles by its direct interaction with the IFT component IFT-54 (DYF-11). After docking of IFT particles, the ciliary pore complex (CPC), a proposed nuclear pore complex (NPC)-like structure[11, 51, 52, 53], might remodel and facilitate the import of assembled IFT particles. Many interesting questions still remain: does FBF1 (DYF-19) and/or TFs determine the ciliary entry of other ciliogenic proteins, such as sensory receptors and signaling molecules? What is the identity of the redundant TF component that regulates the ciliary entry of IFT-B components in DYF-19-deficient cilia? What is the correlation between TF malfunction and ciliopathies? The molecular exploration of TFs is still in its infancy. Current and future studies of the FBF1 (DYF-19) pathway will not only reveal the molecular identity of TFs but also contribute significantly to our understanding of how TFs define the cilium as a functionally and structurally distinct sensory organelle.

## Methods

### Strains

Strains used in this study are listed in Supplementary Table S1. Standard conditions were used to culture and maintain worms. Standard genetic crosses were used to introduce reporter transgenes from wild-type worms into mutant worms. *Jhu455* and *jhu546* mutants were isolated during an EMS screening for dye-filling-defect mutants. Standard single-nucleotide polymorphism mapping was used to clone the mutation. Nonsense mutations at nt880 and nt1219 of the Y43F8C.4 coding region were discovered in *jhu455* and *jhu546*, respectively. Before phenotypic analyses and the introduction of markers, mutants were outcrossed six times against the N2 wild-type.

### Antibodies and reagents

Primary antibodies used in this study include the following: mouse monoclonal antibodies against Odf2 (1A1, Novus, H00004957-M01, 1:400), acetylated tubulin (6-11B-1, Sigma, T7451, 1:400), γ-tubulin (GTU-88, Sigma, T5326, 1:400), polyglutamylated tubulin (GT335, AdipoGen, AG-20B-0020-C100, 1:400), Flag (clone M2, Sigma, F1804, 1:1,000), His (clone HIS.H8, Millipore, 1:1,000), and actin (AC-15, Sigma, A1978, 1:1,000); rabbit

polyclonal antibodies against Cep164 (Sigma, SAB3500022, 1:400), FBF1 (Proteintech, 11531-1-AP, 1:400), IFT88 (Proteintech, 13967-1-AP, 1:400), and IFT140 (Proteintech, 1740-1-AP, 1:400); mouse polyclonal antibody against IFT54 (Abcam ab68958, 1:400); and goat polyclonal antibody against Rootletin (C-20, Santa Cruz, sc-67824, 1:400). All secondary antibodies (goat anti-mouse; rabbit or donkey anti-mouse; rabbit or goat conjugated with Alex Fluor 488, 555, or 647) were purchased from Invitrogen.

### Statistics

Significant differences were identified by the Student's *t*-test (*$P$<0.001). Error bars indicate s.d. For the worm study, *n*=300 animals; 5 independent experiments were performed. For the cell study, *n*=200 cells; 3 independent experiments were performed.

### EMS mutagenesis screen and dye-filling assay

N2 animals were mutagenized with ethyl methanesulfonate (EMS) using standard procedures. F2 progeny from mutagenized animals were grown at 20 °C, and adult animals were incubated in diluted DiI dye (Molecular Probes, 1:200 dilution in M9 of the 2 mg/ml stock in dimethyl formamide) for 1 h at room temperature. After incubation, the animals were washed at least three times with M9 and observed using a fluorescence microscope (M2Bio, Zeiss). Worms that showed defective dye filling were selected.

### Microscopy and imaging

Live, healthy adult worms were anesthetized in 10 mM levamisole and mounted on 5% agarose pads. Images were acquired using either an imaging microscope (Nikon TE 2000-U) with a Plan Apochromat 60x 1.49 oil objective (Nikon) or a Zeiss LSM 780 confocal laser-scanning microscope equipped with a Plan Apochromat 100x oil-immersion objective. Motility stacks were recorded using a CCD camera (Photometrics QuantEM 512SC; Roper Scientific), and kymographs were produced with Metamorph software.

### Transmission electron microscopy (TEM)

TEM on worm amphid cilia was performed as described previously[54]. Briefly, worms were washed and then fixed in 2.5% glutaraldehyde in cacodylate buffer. To facilitate fixation, worm heads were cut off using a syringe needle. Animals were rinsed and then post-fixed with 1% osmium tetroxide in cacodylate buffer for 1 h at 4 °C. Worm heads were oriented and embedded in agarose and then dehydrated and embedded in Embed812 resin according to standard procedures [55]. Thin sections from the anterior tip of the worm head were collected on a diamond knife and post-stained before viewing on an electron microscope (JEM-1400; JEOL).

### Immuno-electron microscopy (immuno-EM)

For pre-embedding immuno-EM, centrosomes were isolated from U2OS cells, fixed with 4% formaldehyde for 20 min, and permeabilized with PBS + 0.1% Triton X-100 for 30 minutes. Blocking and primary antibody incubations were then performed, followed by incubation with goat anti–rabbit IgG-Nanogold. Nanogold was silver-enhanced with HQ

Silver (Nanoprobes), and samples were further processed using standard methods by the EM core facility at Mayo Clinic, Rochester.

### Cell culture and siRNA

Human telomerase-immortalized retinal-pigmented epithelial cells (hTERT RPE-1) and mouse inner medullar collecting duct cells (IMCD3) were cultured in DMEM/F12 supplemented with 10% FBS. HEK293 cells were grown in DMEM with 10% fetal bovine serum. To induce cilia formation, cells were starved for 24–48 h in media without serum after they were grown to confluence.

Mouse *Fbf1* (NM_172571) was used for all subcloning purposes. FLAG-HA double-tagged FBF1 plasmids were transfected into cells using Lipofectamine 2000 (Invitrogen). To obtained RPE or IMCD3 clones stably expressing FBF1 in the centrosome, single cell clones with a lower expression level were selected.

To knock down FBF1, RPE cells were transfected with 50 nM siRNA using Lipofectamine RNAiMAX (Invitrogen) following the manufacturer's instructions. Two consecutive siRNA transfections at a 72-h interval were performed. siRNA sequences targeting human Fbf1 (5′-TGAACAGTTCTTCCTGGAG-3′ and 5′-CCGAGGAGGTGGAGAGCAT-3′) were used.

### Immunofluorescence

For centrosome staining, cells were fixed in −20 °C methanol for 20 min, then blocked in 3% BSA and sequentially incubated with primary and secondary antibodies. For cilia staining, cells were typically fixed with 4% paraformaldehyde for 20 min at room temperature, followed by permeabilization with 0.2% Triton X-100 for 10 min. Cells were then blocked in 3% BSA and sequentially incubated with primary and secondary antibodies.

To stain cilia using the IFT140 antibody, we used an enhanced immunofluorescence protocol[56]. Cells were prefixed with 0.4% paraformaldehyde for 5 min at 37 °C, extracted with 0.5% Triton X-100 in PHEM (50 mM PIPES, 50 mM HEPES, 10 mM EGTA and 10 mM MgCl2, pH 6.9) for 2 min at 37 °C, and then stained following the immunofluorescence procedure described above.

### Immunoprecipitation and GST pull-down

Immunoprecipitation and GST pull-down were performed as described previously[57]. Briefly, HEK293 cells or HEK293 cells expressing double-tagged FLAG-HA FBF1 were lysed in lysis buffer (25 mM Tris-HCl, pH 7.4, 150 mM NaCl, 0.5% NP-40, 1 mM EDTA, and protease inhibitors). The lysate was centrifuged for 20 min at 12,000*g* at 4 °C, and then the supernatant was precleared with protein G Sepharose beads for 4 h. After removal of protein G, the supernatant was incubated with protein G beads and 2 μg of either anti-IFT54 (Abcam) or mouse IgG (Santa Cruz) overnight at 4 °C. After washing the beads five times, the immunocomplexes were separated by SDS–PAGE gels and analyzed.

For GST pull-down assays, pET28a and pGEX-4T-1 constructs were transformed into BL21 (DE3) (Novagen). Proteins were expressed and purified using His resin or glutathione sepharose. Purified His-DYF-11, His-IFT54, or their truncations were incubated with GST,

GST-DYF-9, GST-FBF1, or their truncations immobilized on glutathione sepharose in the binding buffer (25 mM Tris-HCl, pH 7.4, 150 mM NaCl, 0.5% Triton X-100, 1 mM DTT, 10% glycerol, and protease inhibitors) for 4 h at 4 °C. The beads were then washed five times with binding buffer and analyzed by western blot.

### Bimolecular fluorescence complementation (BiFC) assay

The BiFC assay was used to directly visualize the IFT-A, IFT-B, and BBSome complexes in living worms[47]. The following combinations were used in this study: the IFT-A component CHE-11::VN173 with the IFT-B component IFT-20::VC155; the IFT component VC155::DYF-2 with the BBSome component VN173::BBS-9; and the BBSome components VN173::BBS-9 and VC::BBS-7. To examine the BiFC signals relative to the TZ, plasmids in these combinations were co-injected along with the TZ marker MKS-5::mCherry and the co-injection marker pRF4 (rol-6(su1006)) into wild-type worms (5 ng $\mu l^{-1}$ for each BiFC plasmid and MKS-5 vector, 100 ng $\mu l^{-1}$ pRF4). Once a stable line was obtained, the same transgene was crossed into various mutants. Fluorescent signals were visualized by using the YFP filter.

## Supplementary Material

Refer to Web version on PubMed Central for supplementary material.

## Acknowledgments

## References

1. Singla V, Reiter JF. The primary cilium as the cell's antenna: signaling at a sensory organelle. Science. 2006; 313:629–633. [PubMed: 16888132]

2. Goetz SC, Anderson KV. The primary cilium: a signalling centre during vertebrate development. Nat Rev Genet. 2010; 11:331–344. [PubMed: 20395968]

3. Hildebrandt F, Benzing T, Katsanis N. Ciliopathies. N Engl J Med. 2011; 364:1533–1543. [PubMed: 21506742]

4. Badano JL, Mitsuma N, Beales PL, Katsanis N. The ciliopathies: an emerging class of human genetic disorders. Annu Rev Genomics Hum Genet. 2006; 7:125–148. [PubMed: 16722803]

5. Hao L, Scholey JM. Intraflagellar transport at a glance. J Cell Sci. 2009; 122:889–892. [PubMed: 19295122]

6. Pedersen LB, Rosenbaum JL. Intraflagellar transport (IFT) role in ciliary assembly, resorption and signalling. Curr Top Dev Biol. 2008; 85:23–61. [PubMed: 19147001]

7. Rosenbaum JL, Witman GB. Intraflagellar transport. Nat Rev Mol Cell Biol. 2002; 3:813–825. [PubMed: 12415299]

8. Ishikawa H, Marshall WF. Ciliogenesis: building the cell's antenna. Nat Rev Mol Cell Biol. 2011; 12:222–234. [PubMed: 21427764]

9. Qin H, Diener DR, Geimer S, Cole DG, Rosenbaum JL. Intraflagellar transport (IFT) cargo: IFT transports flagellar precursors to the tip and turnover products to the cell body. J Cell Biol. 2004; 164:255–266. [PubMed: 14718520]

10. Fowkes ME, Mitchell DR. The role of preassembled cytoplasmic complexes in assembly of flagellar dynein subunits. Mol Biol Cell. 1998; 9:2337–2347. [PubMed: 9725897]

11. Kee HL, Dishinger JF, Blasius TL, Liu CJ, Margolis B, Verhey KJ. A size-exclusion permeability barrier and nucleoporins characterize a ciliary pore complex that regulates transport into cilia. Nat Cell Biol. 2012; 14:431–437. [PubMed: 22388888]

12. Lin YC, et al. Chemically inducible diffusion trap at cilia reveals molecular sieve-like barrier. Nat Chem Biol. 2013; 9:437–443. [PubMed: 23666116]

13. Reiter JF, Blacque OE, Leroux MR. The base of the cilium: roles for transition fibres and the transition zone in ciliary formation, maintenance and compartmentalization. EMBO Rep. 2012; 13:608–618. [PubMed: 22653444]

14. Anderson RG. The three-dimensional structure of the basal body from the rhesus monkey oviduct. J Cell Biol. 1972; 54:246–265. [PubMed: 5064817]

15. Gilula NB, Satir P. The ciliary necklace. A ciliary membrane specialization. J Cell Biol. 1972; 53:494–509. [PubMed: 4554367]

16. Czarnecki PG, Shah JV. The ciliary transition zone: from morphology and molecules to medicine. Trends Cell Biol. 2012; 22:201–210. [PubMed: 22401885]

17. Sang L, et al. Mapping the NPHP-JBTS-MKS protein network reveals ciliopathy disease genes and pathways. Cell. 2011; 145:513–528. [PubMed: 21565611]

18. Chih B, et al. A ciliopathy complex at the transition zone protects the cilia as a privileged membrane domain. Nat Cell Biol. 2012; 14:61–72. [PubMed: 22179047]

19. Garcia-Gonzalo FR, et al. A transition zone complex regulates mammalian ciliogenesis and ciliary membrane composition. Nat Genet. 2011; 43:776–784. [PubMed: 21725307]

20. Williams CL, et al. MKS and NPHP modules cooperate to establish basal body/transition zone membrane associations and ciliary gate function during ciliogenesis. J Cell Biol. 2011; 192:1023–1041. [PubMed: 21422230]

21. Craige B, et al. CEP290 tethers flagellar transition zone microtubules to the membrane and regulates flagellar protein content. J Cell Biol. 2010; 190:927–940. [PubMed: 20819941]

22. Jauregui AR, Nguyen KC, Hall DH, Barr MM. The Caenorhabditis elegans nephrocystins act as global modifiers of cilium structure. J Cell Biol. 2008; 180:973–988. [PubMed: 18316409]

23. Deane JA, Cole DG, Seeley ES, Diener DR, Rosenbaum JL. Localization of intraflagellar transport protein IFT52 identifies basal body transitional fibres as the docking site for IFT particles. Curr Biol. 2001; 11:1586–1590. [PubMed: 11676918]

24. Graser S, et al. Cep164, a novel centriole appendage protein required for primary cilium formation. J Cell Biol. 2007; 179:321–330. [PubMed: 17954613]

25. Tanos BE, et al. Centriole distal appendages promote membrane docking, leading to cilia initiation. Genes Dev. 2013; 27:163–168. [PubMed: 23348840]

26. Joo K, et al. CCDC41 is required for ciliary vesicle docking to the mother centriole. Proc Natl Acad Sci U S A. 2013; 110:5987–5992. [PubMed: 23530209]

27. Schmidt KN, Kuhns S, Neuner A, Hub B, Zentgraf H, Pereira G. Cep164 mediates vesicular docking to the mother centriole during early steps of ciliogenesis. J Cell Biol. 2012; 199:1083–1101. [PubMed: 23253480]

28. Hedgecock EM, Culotti JG, Thomson JN, Perkins LA. Axonal guidance mutants of Caenorhabditis elegans identified by filling sensory neurons with fluorescein dyes. Developmental biology. 1985; 111:158–170. [PubMed: 3928418]

29. Schmidt T, Karsunky H, Frass B, Baum W, Denzel A, Moroy T. A novel protein (Fbf-1) that binds to CD95/APO-1/FAS and shows sequence similarity to trichohyalin and plectin. Biochim Biophys Acta. 2000; 1493:249–254. [PubMed: 10978533]

30. Sugimoto M, et al. The keratin-binding protein Albatross regulates polarization of epithelial cells. J Cell Biol. 2008; 183:19–28. [PubMed: 18838552]

31. Jakobsen L, et al. Novel asymmetrically localizing components of human centrosomes identified by complementary proteomics methods. Embo J. 2011; 30:1520–1535. [PubMed: 21399614]

32. Kaplan OI, et al. Endocytosis genes facilitate protein and membrane transport in C. elegans sensory cilia. Curr Biol. 2012; 22:451–460. [PubMed: 22342749]

33. Williams CL, Winkelbauer ME, Schafer JC, Michaud EJ, Yoder BK. Functional redundancy of the B9 proteins and nephrocystins in Caenorhabditis elegans ciliogenesis. Mol Biol Cell. 2008; 19:2154–2168. [PubMed: 18337471]

34. Williams CL, Masyukova SV, Yoder BK. Normal ciliogenesis requires synergy between the cystic kidney disease genes MKS-3 and NPHP-4. J Am Soc Nephrol. 2010; 21:782–793. [PubMed: 20150540]

35. Warburton-Pitt SR, Jauregui AR, Li C, Wang J, Leroux MR, Barr MM. Ciliogenesis in Caenorhabditis elegans requires genetic interactions between ciliary middle segment localized NPHP-2 (inversin) and transition zone-associated proteins. J Cell Sci. 2012; 125:2592–2603. [PubMed: 22393243]

36. Pazour GJ, Wilkerson CG, Witman GB. A dynein light chain is essential for the retrograde particle movement of intraflagellar transport (IFT). The Journal of cell biology. 1998; 141:979–992. [PubMed: 9585416]

37. Pazour GJ, Dickert BL, Witman GB. The DHC1b (DHC2) isoform of cytoplasmic dynein is required for flagellar assembly. The Journal of cell biology. 1999; 144:473–481. [PubMed: 9971742]

38. Signor D, et al. Role of a class DHC1b dynein in retrograde transport of IFT motors and IFT raft particles along cilia, but not dendrites, in chemosensory neurons of living Caenorhabditis elegans. The Journal of cell biology. 1999; 147:519–530. [PubMed: 10545497]

39. Wicks SR, de Vries CJ, van Luenen HG, Plasterk RH. CHE-3, a cytosolic dynein heavy chain, is required for sensory cilia structure and function in Caenorhabditis elegans. Developmental biology. 2000; 221:295–307. [PubMed: 10790327]

40. Piperno G, Siuda E, Henderson S, Segil M, Vaananen H, Sassaroli M. Distinct mutants of retrograde intraflagellar transport (IFT) share similar morphological and molecular defects. The Journal of cell biology. 1998; 143:1591–1601. [PubMed: 9852153]

41. Schafer JC, Haycraft CJ, Thomas JH, Yoder BK, Swoboda P. XBX-1 encodes a dynein light intermediate chain required for retrograde intraflagellar transport and cilia assembly in Caenorhabditis elegans. Molecular biology of the cell. 2003; 14:2057–2070. [PubMed: 12802075]

42. Loktev AV, et al. A BBSome subunit links ciliogenesis, microtubule stability, and acetylation. Developmental cell. 2008; 15:854–865. [PubMed: 19081074]

43. Nachury MV, et al. A core complex of BBS proteins cooperates with the GTPase Rab8 to promote ciliary membrane biogenesis. Cell. 2007; 129:1201–1213. [PubMed: 17574030]

44. Lechtreck KF, et al. Cycling of the signaling protein phospholipase D through cilia requires the BBSome only for the export phase. J Cell Biol. 2013; 201:249–261. [PubMed: 23589493]

45. Lechtreck KF, et al. The Chlamydomonas reinhardtii BBSome is an IFT cargo required for export of specific signaling proteins from flagella. J Cell Biol. 2009; 187:1117–1132. [PubMed: 20038682]

46. Ou G, Blacque OE, Snow JJ, Leroux MR, Scholey JM. Functional coordination of intraflagellar transport motors. Nature. 2005; 436:583–587. [PubMed: 16049494]

47. Wei Q, Zhang Y, Li Y, Zhang Q, Ling K, Hu J. The BBSome controls IFT assembly and turnaround in cilia. Nat Cell Biol. 2012; 14:950–957. [PubMed: 22922713]

48. Hu CD, Chinenov Y, Kerppola TK. Visualization of interactions among bZIP and Rel family proteins in living cells using bimolecular fluorescence complementation. Molecular cell. 2002; 9:789–798. [PubMed: 11983170]

49. Li C, et al. An essential role for DYF-11/MIP-T3 in assembling functional intraflagellar transport complexes. PLoS Genet. 2008; 4:e1000044. [PubMed: 18369462]

50. Satir P, Christensen ST. Overview of structure and function of mammalian cilia. Annu Rev Physiol. 2007; 69:377–400. [PubMed: 17009929]

51. Dishinger JF, et al. Ciliary entry of the kinesin-2 motor KIF17 is regulated by importin-beta2 and RanGTP. Nat Cell Biol. 2010; 12:703–710. [PubMed: 20526328]

52. Hurd TW, Fan S, Margolis BL. Localization of retinitis pigmentosa 2 to cilia is regulated by Importin beta2. J Cell Sci. 2011; 124:718–726. [PubMed: 21285245]

53. Ounjai P, et al. Architectural insights into a ciliary partition. Curr Biol. 2013; 23:339–344. [PubMed: 23375896]

54. Li Y, Wei Q, Zhang Y, Ling K, Hu J. The small GTPases ARL-13 and ARL-3 coordinate intraflagellar transport and ciliogenesis. J Cell Biol. 2010; 189:1039–1051. [PubMed: 20530210]

55. Hall DH. Electron microscopy and three-dimensional image reconstruction. Methods Cell Biol. 1995; 48:395–436. [PubMed: 8531736]

56. Jin H, et al. The conserved Bardet-Biedl syndrome proteins assemble a coat that traffics membrane proteins to cilia. Cell. 2010; 141:1208–1219. [PubMed: 20603001]

57. Li Y, Zhang Q, Wei Q, Zhang Y, Ling K, Hu J. SUMOylation of the small GTPase ARL-13 promotes ciliary targeting of sensory receptors. J Cell Biol. 2012; 199:589–598. [PubMed: 23128241]
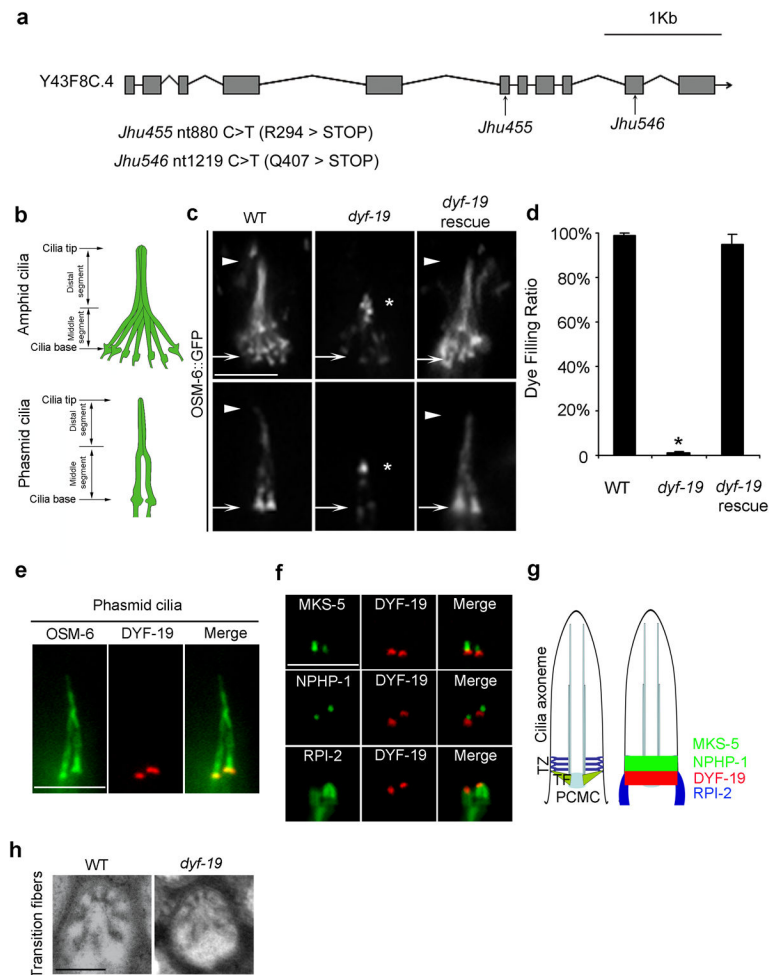
**Figure 1. DYF-19 is a functional component of TFs**

**a,** Schematic of Y43F8C.4 alleles. *Jhu455* and *jhu546* were retrieved from a genome-wide mutagenesis screen for ciliogenesis mutants. *Jhu455* and *jhu546* exhibit identical mutant phenotypes in all experiments we conducted. Hereafter, the *jhu455* allele with an R294>Stop mutation is the reference allele used in this report. **b,** In *C. elegans*, the head amphids and tail phasmids are ciliated neurons and primary sensory organs. The amphid cilia consist of a bundle of 10 cilia, and the phasmid has 2 cilia. **c,** Fluorescence micrographs of cilia labeled with the GFP-tagged IFT-B component OSM-6 in *Wt, dyf-19(jhu455) and dyf-19* rescue strain. *dyf-19* show truncated cilia and abnormal accumulation of OSM-6::GFP at the tips of residual cilia. Arrows and arrowheads indicate the base and tip of cilia, respectively. Stars note the accumulation of OSM-6::GFP. **d,** The dye-filling defect in *dyf-19(jhu455)* is fully rescued by introducing a wild-type copy of the *Y43F8C.4* gene. Data are represented as mean of 5 independent experiments (n=300) and error bars indicate s.d. Significant differences were identified by the Student's *t*-test. *$P$<0.001. **e,** mCherry-tagged DYF-19 specifically localizes at the ciliary base. **f,** Spatial relationships between DYF-19 and TZ markers (MKS-5 and NPHP-1) and between DYF-19 and a PCMC marker (RPI-2)**. g,** Cartoon illustrating the TF localization of DYF-19 at the ciliary base. **h,** Transmission

electron microscopy reveals that *dyf-19* mutants possess normal TFs. Scale bars: 200 nm in **h** and 5 μm in other micrographs.
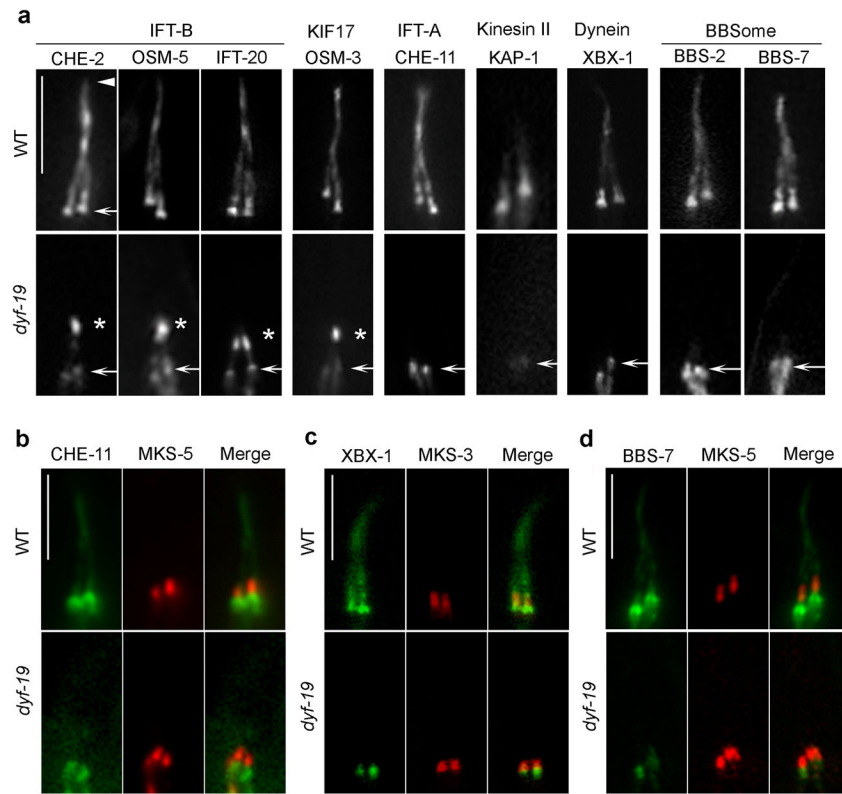
**Figure 2. The ciliary entry of IFT components is compromised in *dyf-19* mutants**

**a,** Fluorescence micrographs of cilia labeled with various IFT markers. In *dyf-19,* IFT-B components (OSM-5, CHE-2, IFT-20) and IFT-B–associated kinesin motor OSM-3/KIF17 show consistent ciliary tip accumulation similar to OSM-6 (Fig. 1c). In contrast, IFT-A components CHE-11, IFT-A–associated kinesin-II subunit KAP-1, dynein light chain XBX-1, and BBSome proteins are all excluded from the cilia. Arrows and arrowheads indicate the base and tip of cilia, respectively. Stars note accumulation. Co-labeling with TZ markers revealed that CHE-11 (**b**), XBX-1 (**c**), and BBS-7 (**d**) were restricted below the TZ in *dyf-19* mutants. Scale bars, 5 μm.
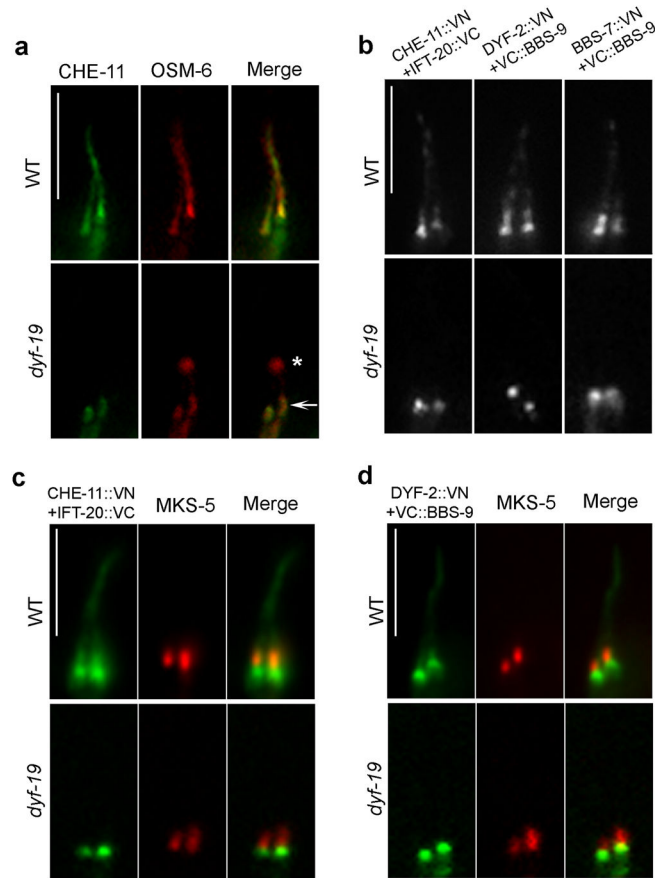
**Figure 3. DYF-19 regulates the ciliary entry of assembled IFT particles**

**a,** At the base of *Wt* or *dyf-19* cilia, the IFT-A component CHE-11 and the IFT-B component OSM-6 colocalize, presumably below the TZ. **b,** In BiFC analyses, fluorescence complementation of CHE-11::VN-IFT-20::VC, DYF-2::VN-VC::BBS-9, and DYF-2::VN-VC::BBS-9 occurs along the entire cilium in *Wt*, but only at the ciliary base in *dyf-19* mutants. Reconstituted CHE-11::VN-IFT-20::VC (**c**) and DYF-2::VN-VC::BBS-9 (**d**) localize just below the TZ marker in *dyf-19* mutants. VN: N-terminus of Venus YFP; VC: C-terminus of Venus YFP. Bars**,** 5 μm.
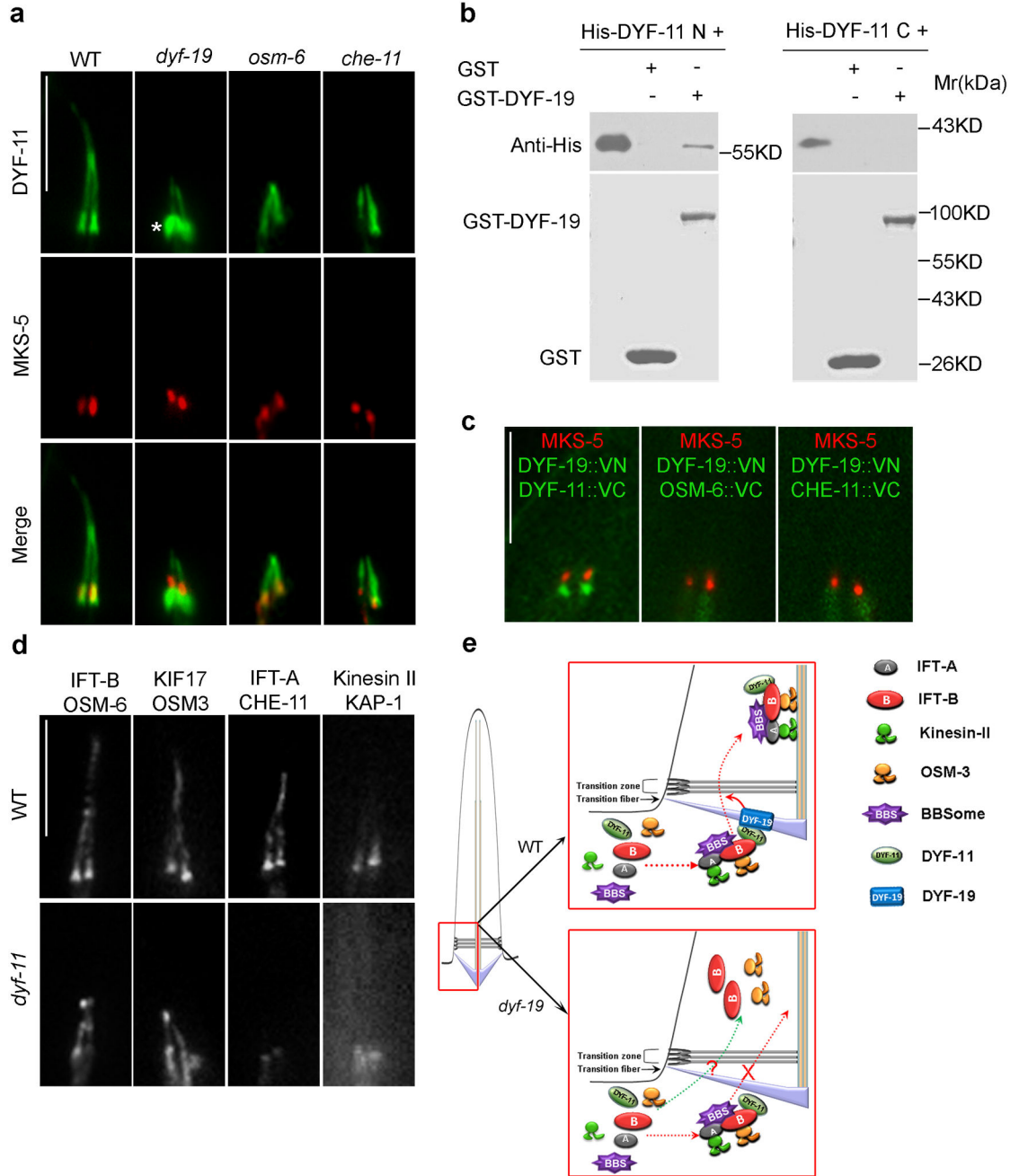
**Figure 4. DYF-19 interacts directly with IFT component DYF-11**

**a,** DYF-11 shows a unique mislocalization pattern in DYF-19-deficient cilia. **b,** The DYF-11 N-terminus interacts directly with DYF-19 in a GST pull-down assay. **c,** At the ciliary base, stable fluorescence complementation in BiFC assays occurs between DYF-19 and DYF-11 but no or very weak between DYF-19 and other IFT components below the TZ. **d,** D*yf-11* mutants show similar phenotypes to *dyf-19* mutants for the ciliary entry of IFT components. **e,** Schematic of the role of TF component DYF-19 in regulating the ciliary entry of assembled IFT particles through a direct interaction with the IFT component DYF-11. VN: N-terminus of Venus YFP; VC: C-terminus of Venus YFP. Bars**,** 5 μm.
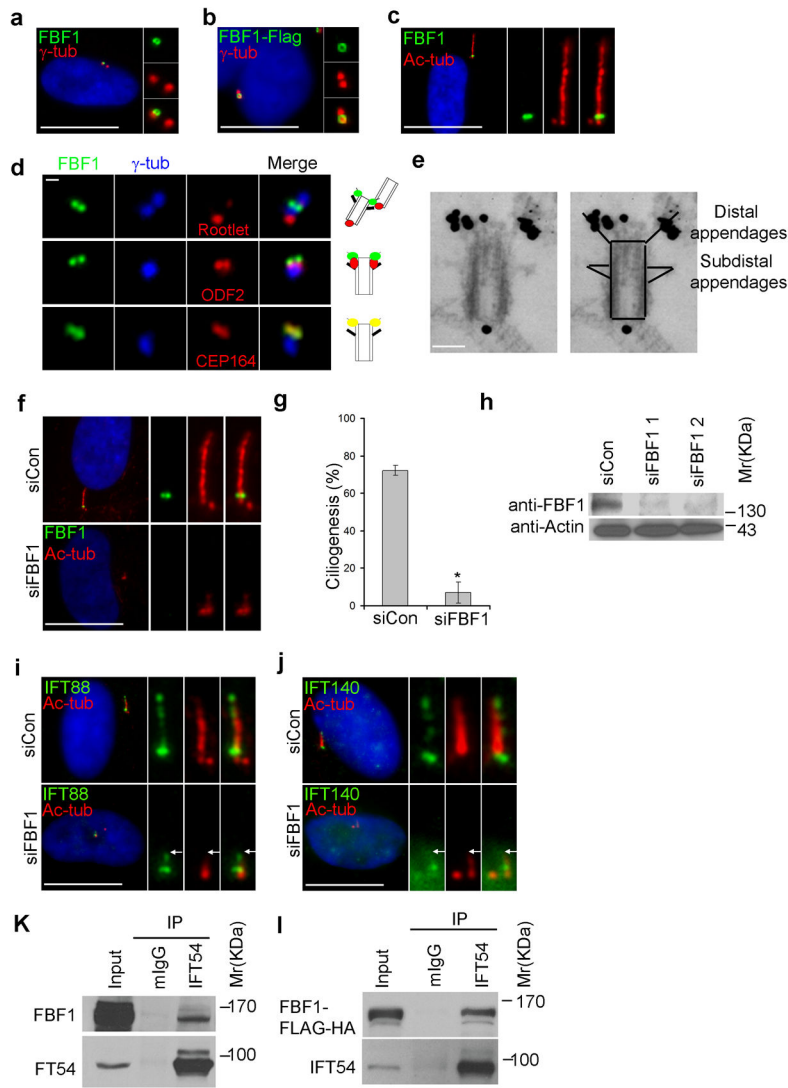
**Figure 5. The localization and function of DYF-19 are highly conserved**
Either endogenous (**a**) or overexpressed (**b**) FBF1, the mammalian homolog of worm DYF-19, localizes specifically on one centriole with a ring-like pattern in IMCD3 cells. **c,** FBF1 localizes at the ciliary base, above the basal body. **d,** In IMCD3 cells, FBF1 localizes above rootlet and subdistal appendage protein ODF2 and completely colocalizes with distal appendage protein CEP164. **e,** Immuno-EM demonstrates that FBF1 localizes specifically to distal appendages of mother centrioles. **f–h,** Knock-down of FBF1 leads to severely truncated cilia in most RNAi-treated hTERT-RPE cells. Data are represented as mean of 3 independent experiments (n=200) and error bars indicate s.d. Significant differences were identified by the Student's $t$-test. *$P<0.001$. **i** and **j,** The IFT-B component IFT88, but not the IFT-A component IFT140, enters the truncated cilia of FBF1-knockdown hTERT-RPE cells. Arrows indicate the tips of truncated cilia. **k,** Endogenous IFT54 immunoprecipitates with FBF1 in hTERT-RPE cells. **l,** HEK293 cells were transiently transfected with FLAG-HA-tagged FBF1, and 48 hours later, cells were subjected to immunoprecipitation using

normal mouse IgG (mIgG) or anti-IFT54 antibody. 50 μg protein were loaded into each lane. Bars: **c,** 1μm; **e,** 200 nm; others, 20 μm.